Shock Waves (2012) 22:363–379
DOI 10.1007/s00193-012-0375-x

ORIGINAL ARTICLE

A thermochemically derived global reaction mechanism for detonation application

Y. Zhu · J. Yang · M. Sun

Received: 16 October 2011 / Revised: 12 April 2012 / Accepted: 24 April 2012 / Published online: 17 May 2012

Abstract A 4-species 4-step global reaction mechanism for detonation calculations is derived from detailed chemistry through thermochemical approach. Reaction species involved in the mechanism and their corresponding molecular weight and enthalpy data are derived from the real equilibrium properties. By substituting these global species into the results of constant volume explosion and examining the evolution process of these global species under varied conditions, reaction paths and corresponding rates are summarized and formulated. The proposed mechanism is first validated to the original chemistry through calculations of the CJ detonation wave, adiabatic constant volume explosion, and the steady reaction structure after a strong shock wave. Good agreement in both reaction scales and averaged thermodynamic properties has been achieved. Two sets of reaction rates based on different detailed chemistry are then examined and applied for numerical simulations of two-dimensional cellular detonations. Preliminary results and a brief comparison between the two mechanisms are presented. The proposed global mechanism is found to be economic in computation and also competent in description of the overall characteristics of detonation wave. Though only stoichiometric acetylene–oxygen mixture is investigated in this study, the method to derive such a global reaction mechanism possesses a certain generality for premixed reactions of most lean hydrocarbon mixtures.

Keywords Global reaction mechanism · Elementary reaction mechanism · Thermochemical property · Detonation

List of symbols

ρ	Mass density
p	Pressure
T	Temperature
T_0	Reference temperature, $T_0 = 298\,\mathrm{K}$
θ	Natural logarithm of density, $\theta = \ln \rho$
ξ	Reciprocal of temperature, $\xi = 10^3/\mathrm{T}$
t	Time
e	Total energy per unit mass
R_u	Universal gas constant
Ea	Activation energy
H	Mean molar enthalpy
H_i	Molar enthalpy of ith species
W	Mean molecular weight
W_i	Molecular weight of ith species
λ	Mole fraction
$[X]$	Molar concentration of species X
δ	Stoichiometric coefficient
s	Reaction order
K_c	Equilibrium constant
k	Reaction rate constant
Ω	Chemical production rate
χ	Stability parameter

1 Introduction

Chemical kinetic models applied in detonation calculations can be categorized as two types—the elementary reaction mechanism (ERM) and the global reaction mechanism

Communicated by S. Dorofeev.

Y. Zhu · J. Yang (✉)
Department of Modern Mechanics, University of Science and Technology of China, Hefei 230027, China
e-mail: jmyang@ustc.edu.cn

Y. Zhu
e-mail: yujianrd@ustc.edu.cn

M. Sun
Center for Interdisciplinary Research, Tohoku University, Sendai 9808578, Japan

Table 1 Reaction mechanisms for acetylene–oxygen combustion

Reaction mechanism	Species	Reactions	Reference
Lutz	39	154	[1]
Miller–Bowman	53	251	[2]
Konnov	127	1207	[3]
SanDiego	46	235	[4]
Petrova–Williams	37	177	[5]
25-Step short	16	25	[13]
7-Step reduced	11	7	[13]

(GRM). ERM is an aggregate of numbers of molecular-level single-transition-state reactions among real chemical species. This type of mechanism provides the most fundamental and precise chemistry for description of reactive flows. By contrast, GRM contains global reaction steps that are either deduced from elementary chemistry or concluded from experimental measurements. It is often concisely formulated to cover only the bold reaction paths or characteristics.

In Table 1, we show a few known ERMs valid for acetylene–oxygen combustion. The top five are the comprehensive ones that may address a wide range of hydrocarbon fuels [1–5]. To elaborate the very fine chemistry, these mechanisms have to include numerous species and reaction steps. The large amount of species as well as the stiffness of the system basically prevents them from being applied in large scale numerical simulation. Varied techniques have been developed to simplify the complex system thereby, which are of two levels in general. The first level aims to weed out the redundant species and reactions, leading towards a skeletal ERM. Techniques applied on this level include varied types of sensitivity analysis (SA) method [6,7], computational singular perturbation (CSP) method [8,9], directed relation graph (DRG) method and related [10,11], and the optimal elimination method [12]. The second level of simplification proceeds further to condense the skeletal mechanism by carrying out time-scale analysis and enforcing chemical equilibrium on species with fast production rates. Quasi-steady state (QSS) approximation [13,14] is a classical method on this level where species that are minor and nearly steady along reaction are eliminated; other techniques, such as the CSP method [8,9,15] and the intrinsic low-dimensional manifold (ILDM) method [16], introduce mathematics to identify and treat the QSS species systematically. The last two in Table 1 are such simplified mechanisms. The 25-step mechanism is a skeletal ERM deduced from a comprehensive one via SA and experimental validation, whereas the 7-step mechanism is derived from the 25-step mechanism via QSS approximation. By these techniques, it is possible to deduce a complex ERM to moderate size while maintaining the preciseness of chemistry in a narrowed scope.

GRM represents another end of the chemistry simplification. It has two subclasses, i.e. the more realistic one which still employs the elementary species system, and the idealized one whose reaction units are further symbolized with often no clear reference. In a strict sense, mechanisms reduced by canceling out QSS species [13] belong to the first subclass of GRM, as their reaction steps are packs of a series of elementary reactions. Following the 7-step mechanism, Varatharajan and Williams [13] proceeded to derive a two-step GRM for acetylene–oxygen detonation. It was also extended to address a couple of other hydrocarbon fuels [17]. Sichel et al. [18] proposed their two-step GRM for hydrogen–oxygen detonation. Other GRMs with real species like [19,20] have a strong engineering background on flames, and were lately reviewed and revised by Anderson et al. [21].

Idealized GRMs are commonly used in detonation investigations, more specifically for theoretical purposes such as the stability analysis of detonation wave. We shall refer to symbolic reaction units as global species in contrast to the elementary chemical species. The most classical case in this family should be the one-step irreversible reaction model, which considers only two global species, and converts one to another following typically an Arrhenius law [22–25]. This one-step mechanism was found incapable of producing some important features of real combustion chemistry (e.g. chain reactions). An ad hoc extension of it is to set a neutral induction step before the exothermic reaction [26–28], whereby the induction stage and heat-release stage are separately modeled. The same technique was also applied in the two-step mechanism of Sichel et al. [18]. Another well known approach is the three-step mechanism [29–31], which takes into account the chain initiation, branching, and termination processes systematically. For better restoration of the explosion limits, Liang et al. [32] proposed a 4-step mechanism. They continued to raise a 5-step one to examine the effects of radical competition [33]. These works have contributed a lot to the understanding of detonation physics as well as the improvement towards more sophisticated GRMs.

Nevertheless, the tradeoff between preciseness and computational efficiency remains a dilemma in processing and application of chemical kinetic models. The potential extend of reduction of a complex ERM is limited. As reviewed by Lu and Law [34], for small hydrocarbon fuels, the deduced skeletal mechanisms still contain tens of species in general

(e.g. [10,12,13]). Together with the stiff problem, large scale numerical simulation with them remains a tough challenge. Although the mechanism may be further reduced by removing QSS species, the resulted number of species seems to reach a minimum around 10, e.g. methane mechanism with 12 species [8], acetylene with 10 [13] and ethylene with 21 [10], which are still costly for simulations upon normal computer. On the other hand, when a mechanism is reduced towards a solvable size, the chemical details are compromised. For a mechanism with real species in its compact form, say, species less than 10, it is fated that fewer species and reactions will come out with a coarser chemistry as well as a shrinking scope of applicability [34]. Mechanisms reached by QSS type of approximation generally focus on high-temperature regime other than low-temperature regime, and tend to work better in flames other than ignition or detonation. Though maybe acceptable for certain applications, the divergence between outcomes of full mechanisms and GRMs is also notable [13,17,21]. Idealized GRMs deflect from the real chemistry even further. With the highly epitomized reaction schemes and the symbolized global species, most of such GRMs cannot strictly address any reaction in reality.

While there have been plenty of works dedicated to reduce the detailed chemistry and to extend the idealized GRMs, respectively, direct connections between these two threads are fairly weak, despite of the primitive projection of global activation energy on a one-step GRM [35,36]. None of the simplification strategies has considered to substitute families or packs of real species with fewer sets of global species; barely has any tried enduing the symbolic reaction units of GRM with equivalent thermodynamic properties, and mimicking the exact thermochemical paths produced by detailed chemistry. This fact has sparked the basic idea of the present study. That is, to approach the real chemistry with a GRM on basis of thermochemistry.

For detonation, in view of the insufficiency of numerical simulation in quantitative reflection of the complex reality thus far and the vital influence of the mixture chemistry on varied aspects of detonation phenomenon, e.g. ignition [29,31], quenching [37,38], instability [27,28,30,39], structure of wave front [32,33,40], there is always the demand for more accurate but affordable reaction models. Furthermore, the interaction between gas dynamics and chemical reactions is essentially realized by the alteration of the thermodynamic properties of the medium, which makes the thermochemical approach of the real chemistry a straight and rational idea. Such an approach is beneficial as well for detonation investigations, as it may help to bridge the complex reality and the classical theory and models where chemistry is highly idealized [41].

Overall, to serve our particular demand for numerical simulation of acetylene–oxygen detonation, we attempt to construct a simple GRM for this mixture and make it quantitatively comparable to corresponding ERM in both the reaction scales and the overall thermodynamics. We first choose a comprehensive ERM as a reference. With this ERM, chemical equilibrium (CEQ) and adiabatic constant volume explosion (CVE) under varied conditions are calculated. The CEQ results are inspected to set up a system of global species with respective thermodynamic data and an equilibrium constraint. The global species are then deployed to substitute the real elementary species in CVE process. By analyzing and summarizing the evolution history of these global species and their parametric dependence, a reaction scheme and corresponding rates are determined. Preliminary tests on the proposed mechanism in numerical simulation of cellular detonation are carried out at the end.

2 General considerations

2.1 Active mixture properties in Euler system

For a premixed reactive system, the interaction between gas dynamics and the chemical reactions is realized by the alteration of the overall thermodynamic properties of the mixture. The exact properties that are actively involved in such a system need to be clarified. Take, for instance, the one-dimensional Euler equations

$$\frac{\partial}{\partial t}\begin{pmatrix}\rho\\ \rho u\\ \rho e\end{pmatrix}+\frac{\partial}{\partial x}\begin{pmatrix}\rho u\\ \rho u^2+p\\ (\rho e+p)u\end{pmatrix}=0 \tag{1}$$

with total energy

$$\rho e=\rho\frac{H}{W}-p+\frac{1}{2}\rho u^2 \tag{2}$$

and the equation of state (EOS)

$$\frac{p}{\rho}=\frac{R_\mathrm{u}}{W}T \tag{3}$$

where, p, ρ, T are pressure, density and temperature, and H, W are the molar enthalpy and molecular weight, respectively. If the flow is composed of N species with mole fraction λ_i $(i = 1, 2, \ldots, N)$, the averaged W and H can be expressed as

$$W=\sum_{i=1}^{N}(\lambda_i\cdot W_i) \tag{4}$$

$$H=\sum_{i=1}^{N}(\lambda_i\cdot H_i) \tag{5}$$

Generally, W_i are known constants and H_i are known functions of local thermal states. For perfect gas, molar enthalpy is only a function of temperature, $H_i = H_i(T)$.

The above completes a simple gasdynamic system, where the active mixture properties that contribute to the system are clearly given by two quantities, i.e. the averaged molar enthalpy H and averaged molecular weight W. Mixtures with the same $H(T)$ and same W are essentially equivalent in spite of the details on H_i, W_i or λ_i. Chemical reactions influence the flow by changing the mixture composition, e.g. λ_i, and hence again the averaged W and H through Eqs. (4) and (5). Given two sets of reactions that result in the same H and W under any circumstance, these two are indistinguishable from the perspective of overall gas dynamics.

These fundamentals suggest that, a reaction mechanism that produces comparable dynamical effects to a real one does not necessarily replicate all the chemical details as long as the averaged enthalpy and molecular weight are simulated properly.

2.2 Projection of real chemistry on a GRM

From the perspective of a symbolic GRM, for example, the 3-step chain-branching mechanism [29,30],

$$\begin{cases} \text{Chain initiation}: & R \rightarrow Y \\ \text{Chain branching}: & R + Y \rightarrow 2Y \\ \text{Chain termination}: & Y \rightarrow P \end{cases} \tag{6}$$

to match the dynamical effects produced by real chemistry, two basic parts need to be addressed. First, to endue the global species R, Y, and P with adequate thermodynamic data, e.g. molecular weight and molar enthalpy, so that they can by mixing produce all important thermochemical states in the reaction. Second, to model the reaction rates so that they can produce important reaction scales, such as the induction time/length, heat-release time/length, etc.

The 3-step scheme (6) is laid out here for demonstration and for later comparison. It is not proved fit for real detonation chemistry though. Therefore, in practice, the design of reaction scheme and the global species system according to the need is also a crucial task.

2.3 Technical consideration

Accordingly, technical procedures of the current work are outlined as follows.

Step 1: Provide a compact **global species system** that can cover all crucial enthalpy and molecular weight situations produced by real chemistry with acceptable accuracy, including an equilibrium constraint among them. To acquire necessary information, chemical equilibrium (CEQ) of the reaction products with detailed ERM is calculated and investigated. Section 3 will fulfill this part.

The species system derived from CEQ is then at least suitable for calculations of equilibrium flow and the CJ detonation wave. To describe the intermediate state within a reaction process, it can be either enough or not. If it is enough, we proceed to Step 2. Otherwise, more species must be supplemented.

Step 2: Build **reaction paths** among those new species and model their **rates**. For numerical simulations solving fluid dynamics and chemical reaction separately under conservation law, every single reaction step is a segment of adiabatic CVE. Therefore, in this study, the adiabatic CVE under different conditions is computed to produce useful reference data. Afterward, the real elementary species of CVE are substituted by the global species preserving the same averaged thermodynamic properties. Developing traces of those global species are then widely analyzed and summarized to construct a global reaction scheme and related reaction rates. Sections 4 and 5 will fulfill this part.

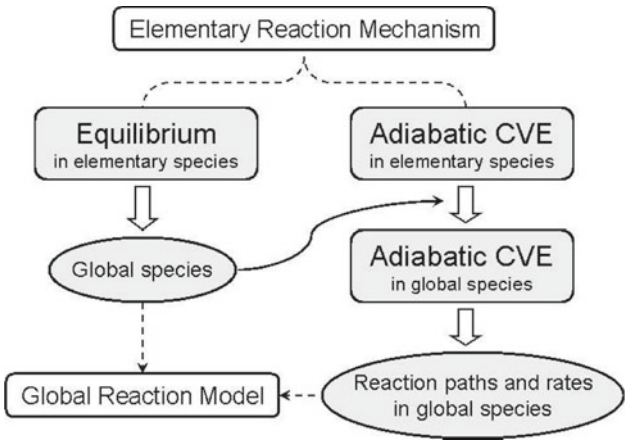

Fig. 1 Technical route to develop a global reaction model from real chemistry

For clarification, a schematic of the procedures discussed above is shown in Fig. 1

3 Global species system

Considering the premixed combustion, a chemical converting path starting from unburned mixture and terminating at equilibrium [18], it will be appropriate to assume at least two global species, one is unburned reactant and the other is the final equilibrium product. This has been the most primitive template taken by many idealized GRMs [22–33,35,36,39]. However, in reality, the equilibrium products of hydrocarbon

combustion vary with ambient condition. When the condition changes significantly, it becomes crucial for a reaction mechanism to involve this equilibrium variation effect. This has directed us to find clues of global species from the thermodynamic properties of equilibrium products.

3.1 Properties of equilibrium products and derivation of global species

Under the restriction of EOS and minimum free-energy criterion, there are only two free variables in determination of equilibrium. Usually, the two take either pressure and temperature (p, T) with minimum Gibbs energy, or density and temperature (ρ, T) with minimum Helmholtz energy. This study employs the latter one. Further more, as discussed in Sect. 2.1, the active thermodynamic properties of the equilibrium products can be fully expressed by the averaged molar enthalpy (H) and molecular weight (W). Together, a four-parameter system—ρ, T, W, H—is employed to investigate the overall equilibrium properties, where the former two serve as independent input variables, and the latter two as output quantities.

The equilibrium is calculated with CHEMKIN EQUIL code [42]. A set of chemical species and corresponding thermodynamic data need to be provided for the calculation. It is found that a collection of species as compact as that of the 25-step mechanism [13] has been sufficient for description of the final equilibrium state of the stoichiometric acetylene–oxygen reaction. Extension of it will not make any sensible difference. The calculation is not as well sensitive to the selection of available thermodynamic data. Despite that, the full 127 species of the Konnov mechanism [3] and its affiliated thermodynamic data have been adopted in current study.

The resulted averaged molecular weight and molar enthalpy of the equilibrium products are shown in Fig. 2. It is obvious that both diagrams present three relatively steady states, and other situations appear like a continuous transition among them. We then attempt to compose proper chemical packs that can produce these steady states equivalently.

The averaged molar enthalpy and molecular weight of a chemical pack can be calculated through Eqs. (4) and (5). For enthalpy, once taking the standard polynomial formula (CHEMKIN format),

$$H_i = H_i(T) = \sum_{k=0}^{m} (a_{ik} \cdot T^k) \tag{7}$$

the averaged enthalpy of the chemical pack can be written in exactly the same form

$$H = \sum_{i=1}^{N} (H_i \cdot \lambda_i) = \sum_{k=0}^{m} (a_k \cdot T^k) \tag{8}$$

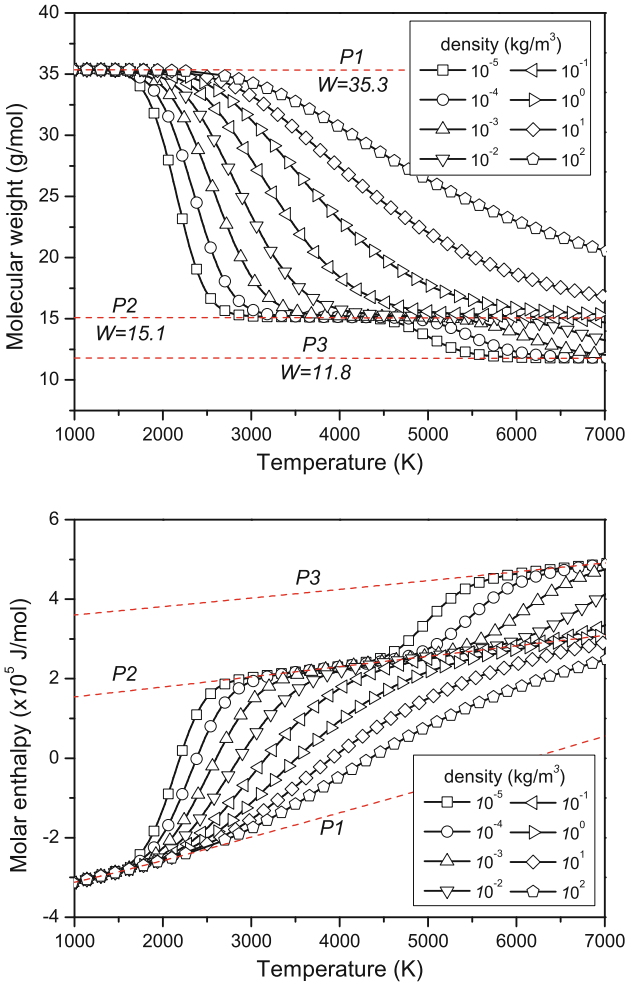

Fig. 2 Averaged molar enthalpy and molecular weight at chemical equilibrium (reaction products of stoichiometric acetylene–oxygen)

with coefficients

$$a_k = \sum_{i=1}^{N} (a_{ik} \cdot \lambda_i) \tag{9}$$

Interestingly, it is found that there are three simple chemical packs—P1, P2, P3,

$$\begin{aligned} 2C_2H_2 + 5O_2 &\dashrightarrow R \\ \rightleftharpoons 4CO_2 + 2H_2O &\dashrightarrow P1 \\ \rightleftharpoons 4CO + 4H + 6O &\dashrightarrow P2 \\ \rightleftharpoons 4C + 4H + 10O &\dashrightarrow P3 \end{aligned} \tag{10}$$

whose enthalpy and molecular weight are nicely matching those steady states (dashed lines in Fig. 2). Noticing that the third pack P3 appears only under extremely high temperature and low density which will not massively exist in normal detonation phenomenon, it is therefore ignored in later discussion and only P1 and P2 are concerned. A further expectation for these chemical packs is to produce by mixing the entire enthalpy and molecular weight maps, plus unburned mixture

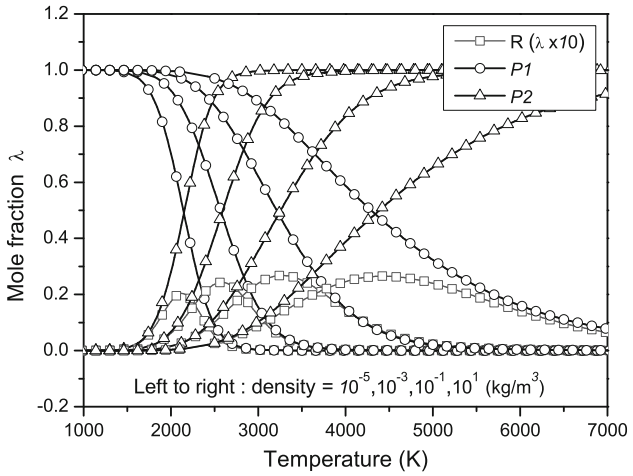

Fig. 3 Mole fractions of three global species at chemical equilibrium (reaction products of stoichiometric acetylene–oxygen)

R if necessary. As long as it works, these chemical packs can be reasonably taken as the global species.

To check this idea, we presume that the equilibrium mixture contains only three global species (R, P1, P2). Their mole fraction λ ($0 \le \lambda \le 1$) for any given ρ and T can then be solved through equation

$$\begin{cases} \lambda_{\mathrm{R}} \cdot W_{\mathrm{R}} + \lambda_{\mathrm{P1}} \cdot W_{\mathrm{P1}} + \lambda_{\mathrm{P2}} \cdot W_{\mathrm{P2}} = W \\ \lambda_{\mathrm{R}} \cdot H_{\mathrm{R}} + \lambda_{\mathrm{P1}} \cdot H_{\mathrm{P1}} + \lambda_{\mathrm{P2}} \cdot H_{\mathrm{P2}} = H \\ \lambda_{\mathrm{R}} + \lambda_{\mathrm{P1}} + \lambda_{\mathrm{P2}} = 1 \end{cases} \tag{11}$$

The derived mole fractions for four representative density cases are plotted in Fig. 3. It shows up that all solutions are smooth to ρ and T and well limited between 0 and 1, perfectly satisfying our presumption. Equilibrium product tends to P2 at higher temperature and lower density, or P1 reversely, which is expected because the gas molecule tends to dissociate when heated or rarefied. Meanwhile, when P1 and P2 coexist, reactant R still remains. Since this R remnant is tiny (less than 3 %, note the amplitude of λ_{R} in Fig. 3 is magnified by a factor of 10), we decide to neglect it by distributing its portion into P1 and P2. Consequently, the real complex of elementary species at equilibrium is replaced by a mixture of only two global species.

3.2 Equilibrium constraint between P1 and P2

A correlation between the equilibrium and the local thermal state need to be set up mathematically to recover the data in Fig. 3. In consistent with the former discussion and for later application as well, mixture density ρ and temperature T are chosen as the two free input variables.

Considering a reversible reaction

$$\mathrm{P1} \rightleftharpoons \delta \cdot \mathrm{P2} \tag{12}$$

the basic thermodynamical approach of the equilibrium state [42] is by

$$\frac{[\mathrm{P2}]_e^{\,\delta}}{[\mathrm{P1}]_e} = (K_{\mathrm{c}})^{1/s} = \exp\left(-\frac{\Delta G}{\mathrm{RT}}\right) \cdot \left(\frac{P_{\mathrm{atm}}}{\mathrm{RT}}\right)^{\delta-1} \tag{13}$$

where, K_{c} represents the equilibrium constant, s the order of forward reaction, and $\Delta G = \delta \cdot G_2 - G_1$ with G_1 and G_2 the Gibbs free energy of P1 and P2, respectively.

However, unlike the enthalpy, the mixture-averaged free energy G_1 and G_2 are found mismatching the real case, and consequently the equilibrium mole fractions derived from Eq. (13) cannot agree with the data in Fig. 3.

The equilibrium correlation must be approached in other ways, thereby. We present here a result of curve fitting which yields an explicit function of mole fraction on total density and temperature, $\lambda = \lambda(\rho, T)$.

Let $\theta = \ln \rho$ and $\xi = 10^3/\mathrm{T}$ (ρ in kg/m^3 and T in K). It is found that the curves for different density in Fig. 3 become rather similar to each other in plane of $\xi - \lambda$. An idea is then to overlap these curves by translation and scaling, whereby the two-variate dependence of λ on ρ and T may be carried by one single variable,

$$\eta = \eta(\rho, T) = \frac{\xi - \xi_c(\theta)}{\varpi(\theta)} \tag{14}$$

Here, ξ_c is the value of ξ when $\lambda = 0.5$, and ϖ is a scaling factor of the width, say, the distance of ξ between $\lambda = 0.2$ and $\lambda = 0.8$. They are both functions of the density or θ.

Fitting ξ_c and ϖ into polynomials of θ results in

$$\eta = \frac{10^2 \cdot \xi - (\alpha_1 + \alpha_2 \cdot \theta)}{\delta_0 + \delta_1 \cdot \theta + \delta_2 \cdot \theta^2} \tag{15}$$

After that, we look forward to model the stepwise dependence of λ on η with a Boltzmann sigmoid function,

$$\lambda = \frac{1}{1 + \exp(\mu \cdot \eta)} \tag{16}$$

For better accuracy, μ is again fitted into a polynomial. And the mole fractions of P1 and P2 at equilibrium are finally formulated.

$$\begin{cases} \lambda_{e\mathrm{P1}} = \dfrac{1}{1 + \exp[-\eta \cdot (\beta_0 + \beta_1 \cdot \eta + \beta_2 \cdot \eta^2)]} \\ \lambda_{e\mathrm{P2}} = 1 - \lambda_{e\mathrm{P1}} \end{cases} \tag{17}$$

Values of the coefficients are given in Table 2.

One may also transfer mole fractions into molar concentrations (for later application) by

$$[X] = \lambda_X \cdot \frac{\rho}{W} \qquad (X = \mathrm{R}, \mathrm{P1}\ or\ \mathrm{P2}) \tag{18}$$

If only the equilibration of P1 and P2 is concerned, it becomes

$$[X]_e = \lambda_{eX} \cdot \frac{\rho_{\mathrm{P1}} + \rho_{\mathrm{P2}}}{\lambda_{e\mathrm{P1}} W_{\mathrm{P1}} + \lambda_{e\mathrm{P2}} W_{\mathrm{P2}}} \tag{19}$$

Table 2 Coefficients for equilibrium relation (units: ρ in kg/m^3, and T in K)

Fuel (C_xH_y)	Hydrogen (H_2)	Methane (CH_4)	Acetylene (C_2H_2)	Propane (C_3H_8)
z	(s) 0.0	(l) 2.0	(s) 0.0	(l) 3.0
α_1	23.8046	24.6368	26.9660	25.0754
α_2	−1.7840	−1.7513	−1.7044	−1.7430
δ_0	13.3542	13.0501	15.7345	13.3145
δ_1	0.1950	0.2536	0.2625	0.2528
δ_2	0.0048	0.0063	0.0048	0.0056
β_0	3.7661	3.7696	3.7136	3.7182
β_1	−0.9971	−0.9962	−1.4730	−0.9940
β_2	0.3901	0.4663	1.0328	0.5705

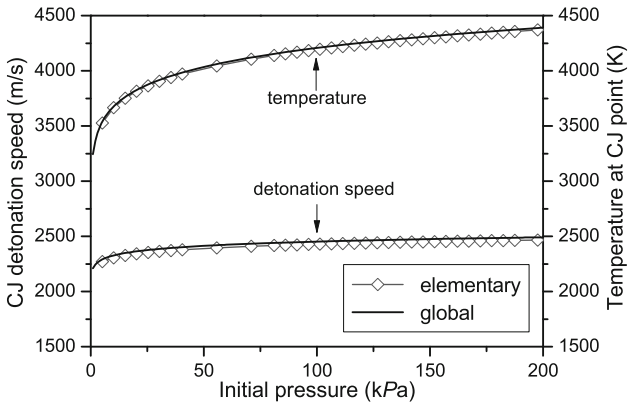

Fig. 4 CJ detonation speed and temperature for stoichiometric acetylene–oxygen mixture

Now a system of three global species with corresponding molecular weight and thermodynamic data, and a constraint of equilibrium dependence on ρ and T is established.

3.3 A simple validation

The CJ detonation problem is calculated to validate above global species system as well as the equilibrium constraint. The problem concerns no chemical reaction paths or speeds, and involves only a conservation law across a discontinuity separating reactant R and products P1 and P2. Two additional conditions are given to close the equations. First, the sonic condition, i.e. $u_{\mathrm{CJ}} = c_{\mathrm{CJ}}$, in wave front frame [41]. Second, P1 and P2 are at chemical equilibrium at the CJ point.

Figure 4 shows the CJ detonation speed and the temperature at the CJ point for stoichiometric acetylene–oxygen mixture. Symbols are those calculated by program GASEQ [43] with elementary species, and lines are results of the current global species. The two are found in good agreement, which indicates that the proposed global species and the fitted equilibrium function are valid for prediction of thermochemistry at chemical equilibrium.

3.4 Generality

The observed molecular and enthalpy characteristics of equilibrium products are rather common for most lean hydrocarbon–oxygen reactions, from which similar sets of global species may be derived. Chemical packs for fuel C_xH_y with $x \geq 0$, $y > 0$ and $z \geq 0$ ($z = 0$: stoichiometric; $z > 0$: lean) can be summarized as

$$\begin{aligned} &C_xH_y + (x + y/4 + z) \cdot O_2 && \dashrightarrow \mathrm{R} \\ &\rightarrow\ x \cdot CO_2 + (y/2) \cdot H_2O + z \cdot O_2 && \dashrightarrow \mathrm{P1} \\ &\rightleftharpoons\ x \cdot CO + y \cdot H + (x + y/2 + 2z) \cdot O && \dashrightarrow \mathrm{P2} \end{aligned} \tag{20}$$

It is also possible to fit the equilibrium proportion with the same formulas as Eqs. (15) and (17). The fitted coefficients for another three sample mixtures are listed in Table 2.

As diluted by inert gases, the equilibrium constraint never changes if one replaces the input total density with the partial density of reactive mixture.

Rich mixtures, however, are found more difficult to deduce into several global species, although they do present some steady states as well. This may be partially ascribed to the remnant of unstable fuel and its complicated dissociation and recombination process.

4 Global reaction scheme

With the proposed global species system, the reaction initial and terminal have been settled.

$$R \longrightarrow \lambda_{e\mathrm{P1}} \cdot \mathrm{P1} + \lambda_{e\mathrm{P2}} \cdot \mathrm{P2} \tag{21}$$

The next objective is to build proper intermediate reaction paths to realize above conversion. This requires a reliable ERM and a standard reaction process to create necessary reference data. Currently, the full Konnov mechanism [3] is adopted as the reference ERM, and the adiabatic CVE process is employed as the test platform. The reaction is integrated with the CHEMKIN CV program [42].

4.1 Adiabatic CVE and replacement of species

For adiabatic CVE, the energy conservation degenerates to

$$e = \frac{H - R_u T}{W} = \frac{H_0 - R_u T_0}{W_0} = \text{Constant} \tag{22}$$

where the subscript 0 denotes the known initial value. Since density ρ is a constant, we have four overall parameters changing along the reaction, i.e. H, W, T and p. Combining with Eqs. (22) and (3), free parameters are only two. When T and p are known, W and H can be easily derived. And once W and H are reproduced alternatively, the presented thermal state T and p will also match the originals. Therefore, to replace the elementary species in reaction with the three global species, we simply follow the same way in Sect. 3.1 trying to match W and H with Eq. (11)

A question we raised in Sect. 2.3 can be answered here. That is whether the three global species derived from CEQ are adequate for description of the intermediate state during reaction. If they are, the solution has to be mathematically and physically appropriate at any point and under any situation. Two typical CVE cases are demonstrated in Fig. 5. The upper figure shows the temperature and pressure profiles from the Konnov mechanism, while the lower shows the mole fractions of R, P1 and P2 derived from upper data. It turns out that the results are quite acceptable. Mole fractions are found smoothly changing and well limited between 0 and 1 throughout the reaction process. This confirms that the three global species are adequate to replace the complicated elementary species involved in the real reaction, with no need of supplementary.

4.2 Global reaction scheme

The reaction features presented in Fig. 5 are typical for premixed hydrocarbon combustion. The reaction process in term of the new global species may be understood as follows.

First, the reaction undergoes an relatively steady stage where mixture properties barely change. The duration of this period is usually referred as induction time. Then the temperature and pressure build up abruptly which forms the main exothermic reaction period. Figure 5 shows that the reactant R converts to P1 and P2 simultaneously till R is almost exhausted. After this, the equilibrating process between P1 and P2 becomes dominant. For current mixture, the final equilibration is endothermic and P1 is converted to P2 gradually leaving a peak in both temperature and pressure profiles.

According to above observations, we try to model the whole reaction with three different regimes. Namely, (a) a neutral induction regime, (b) an irreversible exothermic regime converting R to P1 and P2 separately, and (c) an equilibration regime between P1 and P2. The reaction scheme can

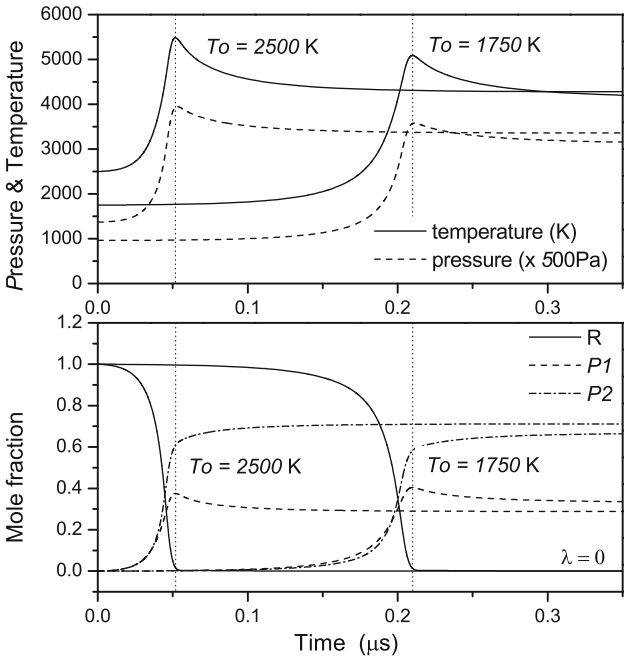

Fig. 5 Examples of adiabatic CVE and the equivalent description of them with three global species for stoichiometric acetylene–oxygen mixture

be written as

$$\begin{cases} \text{(i)} \quad \text{R0} \to \text{R1} & k_i \\ \text{(r1)} \quad \text{R1} \to \delta_1 \cdot \text{P1} & k_{r1} \\ \text{(r2)} \quad \text{R1} \to \delta_2 \cdot \text{P2} & k_{r2} \\ \text{(e)} \quad \text{P1} \rightleftharpoons \delta_3 \cdot \text{P2} & k_{ef}, k_{er} \end{cases} \tag{23}$$

The stoichiometric coefficients are

$$\delta_1 = \frac{W_R}{W_{P1}}, \delta_2 = \frac{W_R}{W_{P2}}, \delta_3 = \frac{W_{P1}}{W_{P2}} = \frac{\delta_2}{\delta_1} \tag{24}$$

For current mixture $\delta_1 = 6/7, \delta_2 = 2, \delta_3 = 7/3$. k_i, k_{r1}, k_{r2} and k_{ef}, k_{er} are the absolute rate constants which rely on the local thermal state only.

To mark the progress of induction, reactant R is divided into two parts, one as the original unactivated one R0 and the other the activated one R1. Both take the same molecular weight and molar enthalpy as R. This extends the previous 3-species system to 4-species one.

It will be beneficial to make a comparison of current mechanism with the 3-step global mechanism described in Sect. 2.2. The activated reactant R1 plays a similar role as the radical Y. Reaction (r1), (r2) and (e) together are an elaboration of the final chain termination step.

To bring in the chain initiation and branching effect as that of the 3-step mechanism, reaction (i) is considered a packed formula of the following two sub-steps,

$$\begin{cases} \text{Initiation} & : \text{R0} \to \text{R1} & k_{i1} \\ \text{Branching} & : \text{R0} + s_0 \cdot \text{R1} \to (1 + s_0) \cdot \text{R1} & k_{i2} \end{cases} \tag{25}$$

Thus the production rate of R0 and R1 yields

$$\frac{d[\mathrm{R1}]}{\mathrm{d}t} = -\frac{d[\mathrm{R0}]}{\mathrm{d}t} = [\mathrm{R0}] \cdot k_{\mathrm{i}1} + [\mathrm{R0}][\mathrm{R1}]^{s_0} \cdot k_{\mathrm{i}2} \tag{26}$$

Letting $k_{\mathrm{i}1}/k_{\mathrm{i}2} = \varepsilon \equiv$ Constant ($\varepsilon \ll 1$), Eq. (26) is further simplified.

$$\frac{d[\mathrm{R1}]}{\mathrm{d}t} = -\frac{d[\mathrm{R0}]}{\mathrm{d}t} = [\mathrm{R0}](\varepsilon + [\mathrm{R1}]^{s_0}) \cdot k_{\mathrm{i}} \tag{27}$$

This form of rate expression has been investigated by Fickiett et al. [22]. In this study, we simply set ε to be 0.001. The overall production rates of the four species in molar concentration then become

$$\begin{cases} \Omega_{\mathrm{R0}} = d[\mathrm{R0}]/\mathrm{d}t = -[\mathrm{R0}](\varepsilon + [\mathrm{R1}]^{s_0}) \cdot k_{\mathrm{i}} \\ \Omega_{\mathrm{r1}} = d[\mathrm{R1}]/\mathrm{d}t = +[\mathrm{R0}](\varepsilon + [\mathrm{R1}]^{s_0}) \cdot k_{\mathrm{i}} \\ \qquad\qquad - ([\mathrm{R1}]^{s_1} \cdot k_{\mathrm{r1}} + [\mathrm{R1}]^{s_2} \cdot k_{\mathrm{r2}}) \\ \Omega_{\mathrm{P1}} = d[\mathrm{P1}]/\mathrm{d}t = [\mathrm{R1}]^{s_1} \cdot k_{\mathrm{r1}} \cdot \delta_1 \\ \qquad\qquad - ([\mathrm{P1}]^{s_3} \cdot k_{\mathrm{ef}} - [\mathrm{P2}]^{s_3\delta_3} \cdot k_{\mathrm{er}}) \\ \Omega_{\mathrm{P2}} = d[\mathrm{P2}]/\mathrm{d}t = [\mathrm{R1}]^{s_2} \cdot k_{\mathrm{r2}} \cdot \delta_2 \\ \qquad\qquad + ([\mathrm{P1}]^{s_3} \cdot k_{\mathrm{ef}} - [\mathrm{P2}]^{s_3\delta_3} \cdot k_{\mathrm{er}}) \cdot \delta_3 \end{cases} \tag{28}$$

where s_1, s_2, s_3 represent the orders of forward reaction of (r1), (r2) and (e), respectively. For reversible reaction (e), the forward rate k_{ef} and reverse rate k_{er} are correlated by the equilibrium constant K_{c}, i.e. $k_{\mathrm{ef}} = K_{\mathrm{c}} \cdot k_{\mathrm{er}}$. K_{c} has been available for any given temperature and density using Eqs. (13) and (19)

In total, to complete the reaction system above, four reaction orders—s_0, s_1, s_2, s_3, and four reaction rates—$k_{\mathrm{i}}, k_{\mathrm{r1}}, k_{\mathrm{r2}}, k_{\mathrm{ef}}$—need to be evaluated.

5 Reaction rates

Adiabatic CVE cases over a wide range of initial temperature and density conditions are tested.

The CJ detonation speed in current mixture is about 2,400 m/s (Fig. 4), corresponding to a Mach number around 7.3. Allowing certain degree of overdrive, the temperature at the Neumann point of a Mach 9.0 detonation is about 3,100 K. Therefore, we will test the initial temperature ranging from 1,000 to 3,500 K. As for density, it is chosen to cover the post state of shock waves with Mach number 1.1−9.0 under initial pressure 10^{-2}−10^{2} atm, which brings to a density scope of 10^{-3}−10^{2} kg/m^3.

5.1 Derivation procedures

Since the molar concentrations of R, P1 and P2 changing along time have been achievable using Eqs. (11) and (18), the changing rates of the the global species can be approximated by

$$\Omega_X \approx \frac{\Delta[X]}{\Delta t} = \frac{[X]^+ - [X]^-}{t^+ - t^-} \quad (X = \mathrm{R}, \mathrm{P1} \text{ or } \mathrm{P2}) \tag{29}$$

Note here only R([R] = [R0] + [R1]) is resolvable while the exact share of R0 and R1 is unclear. We simply assume that when the amounts of P1 and P2 become notable, reaction (i) has almost completed. Thereby [R0] $\simeq$ 0 and [R1] $\simeq$ [R]. Using Eq. (28) reversely with predetermined reaction orders (constants), rates $k_{\mathrm{r1}}, k_{\mathrm{r2}}, k_{\mathrm{ef}}$ and k_{er} can be derived.

Figure 5 shows that when reaction (e) dominates (period behind the vertical dashed lines) the remnant of R tends to zero, which makes the influence from reaction (r1) and (r2) negligible. Therefore, in this period, rate k_{ef} (or k_{er}) can be solely calculated regardless of other reactions,

$$k_{\mathrm{ef}} = -\frac{\Omega_{\mathrm{P1}}}{[\mathrm{P1}]^{s_3} - [\mathrm{P2}]^{s_3\delta_3}/K_{\mathrm{c}}} \tag{30}$$

Similarly, we may extract rate k_{r1} and k_{r2} from the main exothermic period where reaction (r1) and (r2) are dominating and reaction (i) almost terminates. Have k_{ef} and k_{er} been modeled and [R1] $\simeq$ [R], k_{r1} and k_{r2} can be calculated as followed.

$$\begin{cases} k_{\mathrm{r1}} = \dfrac{\Omega_{\mathrm{P1}} + ([\mathrm{P1}]^{s_3} \cdot k_{\mathrm{ef}} - [\mathrm{P2}]^{s_3\delta_3} \cdot k_{\mathrm{er}})}{[\mathrm{R1}]^{s_1} \cdot \delta_1} \\ k_{\mathrm{r2}} = \dfrac{\Omega_{\mathrm{P2}} - ([\mathrm{P1}]^{s_3} \cdot k_{\mathrm{ef}} - [\mathrm{P2}]^{s_3\delta_3} \cdot k_{\mathrm{er}}) \cdot \delta_3}{[\mathrm{R1}]^{s_2} \cdot \delta_2} \end{cases} \tag{31}$$

The induction rate k_{i} is treated at last and specially. Instead of analyzing known molar concentrations, it is evaluated by matching the real induction time.

5.2 Reaction orders and rates

Following above method, the rate data of $k_{\mathrm{ef}}, k_{\mathrm{r1}}$ and k_{r2} are distilled in batches through a processing program. Results are displayed in Figs. 6 and 7 as hollow symbols. In each of these figures, six symbol types correspond to six different total densities ($\rho = 10^a$ kg/m^3, $a = -3, -2, -1, \ldots, 2$), and the data points for each density are from about 45 test cases of initial temperature.

A rough estimation on the reaction order s_1, s_2 and s_3 has been carried out in advance. The criterion for determination of them is to assure the data points from the same density disperse the least, such that the dependence of rate k on ρ and T is purified as much as possible.

For the Konnov mechanism, the three reaction orders yield

$$\begin{cases} s_1 = s_2 = 0.85 \\ s_3 = 1.02 \end{cases} \tag{32}$$

Using those reaction orders, the data present evident regularities. First, points for each density case gather into a narrow strip in the plane of $\ln k$ versus $10^3/T$, and the strip is nearly

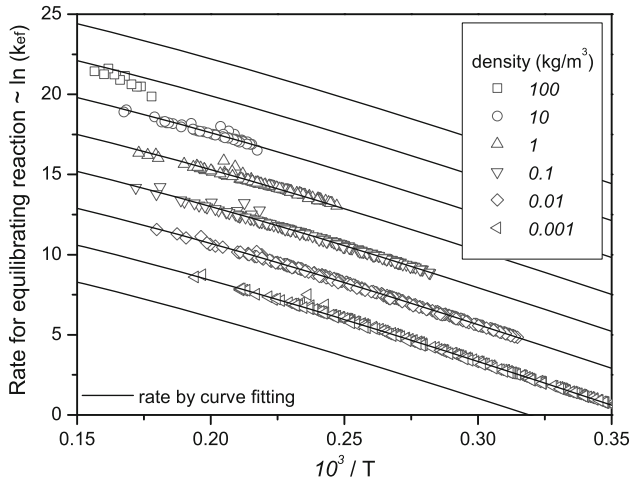

Fig. 6 Rate of forward equilibrating reaction, k_{ef} (for stoichiometric acetylene–oxygen reaction)

straight, which suggests an Arrhenius type rate function. Second, the strips of the six density cases are almost parallel to each other, which suggests $k \propto \rho^m$. Therefore, we attempt to fit those data with the following function.

$$k = A \cdot \rho^m \cdot T^n \cdot \exp\left(-\frac{\mathrm{Ea}}{\mathrm{RT}}\right) \tag{33}$$

The equilibration rate k_{ef} is relatively ease to fit (Fig. 6), which results in a simple equation.

$$k_{\mathrm{ef}} = 1.78 \times 10^{27}\ \rho\ T^{-4} \cdot \exp\left(-\frac{224.3\ \mathrm{RT}_0}{\mathrm{RT}}\right) \tag{34}$$

The two main reaction rates k_{r1} and k_{r2}, however, are far more complicated (Fig. 7). Inspired by the stepwise feature of previous equilibrium properties, we tend to consider the total rate as an integration of two basic rates joined by a transit function. In each figure, there marks a dashed line dividing the rate plane into two regions; and in each region the rate-strips from different densities present evident similarities. By fitting Eq. (33) throughout the regular part of respective regions, one may get two basic rates, i.e. a high-temperature rate k_{H} in the left and a low-temperature rate k_{L} in the right. The total rate then can be assembled as

$$k = \phi \cdot k_{\mathrm{H}} + (1 - \phi) \cdot k_{\mathrm{L}} \tag{35}$$

Similar to Eq. (16), the transit function ϕ applies a Boltzmann sigmoid function

$$\phi = \frac{1}{1 + \exp\left(\mu \cdot (\xi - \xi_c)\right)} \tag{36}$$

where, $\xi = 10^3/T$, ξ_c is the value of ξ when $\phi = 0.5$, and μ controls the transition slop (or width) between two states.

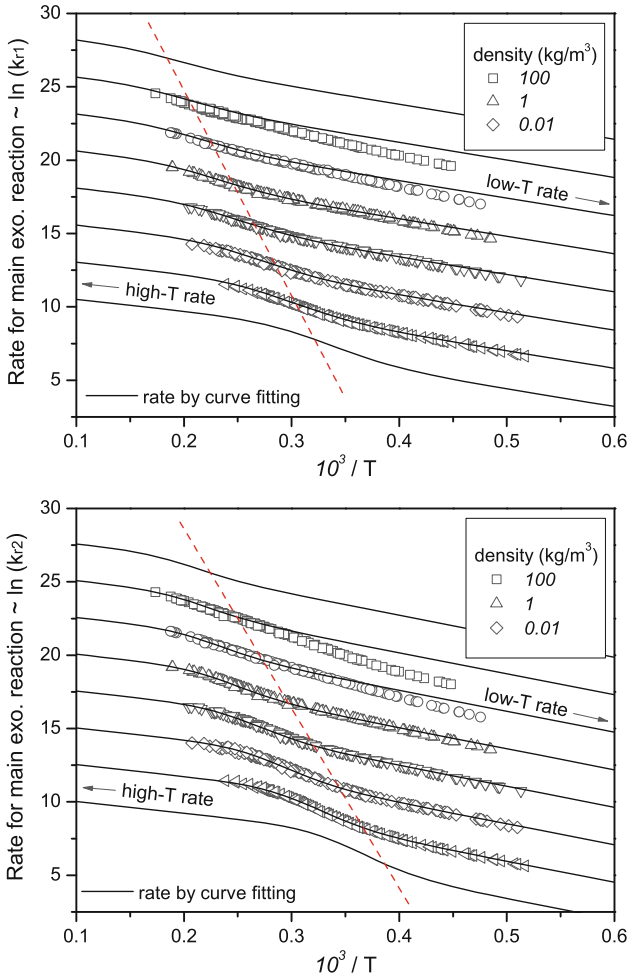

Fig. 7 Rates for main reaction $r1$ and $r2$, k_{r1} *and* k_{k2} (for stoichiometric acetylene-oxygen reaction)

Fitting results are given below.

$$k_{\mathrm{r1}} \begin{cases} k_{\mathrm{r1H}} = 2.05 \times 10^9\ \rho^{1.10} \cdot \exp\left(-\dfrac{26.8\mathrm{RT}_0}{\mathrm{RT}}\right) \\ k_{\mathrm{r1L}} = 1.05 \times 10^9\ \rho^{1.13} \cdot \exp\left(-\dfrac{40.0\mathrm{RT}_0}{\mathrm{RT}}\right) \\ \mu_{\mathrm{r1}} = 35.0\ ; \qquad \xi_{c1} = 0.13 + \dfrac{0.070}{\rho^{0.095}} \end{cases} \tag{37}$$

$$k_{\mathrm{r2}} \begin{cases} k_{\mathrm{r2H}} = 1.15 \times 10^9\ \rho^{1.09} \cdot \exp\left(-\dfrac{26.8\mathrm{RT}_0}{\mathrm{RT}}\right) \\ k_{\mathrm{r2L}} = 1.05 \times 10^9\ \rho^{1.11} \cdot \exp\left(-\dfrac{48.0\mathrm{RT}_0}{\mathrm{RT}}\right) \\ \mu_{\mathrm{r2}} = 44.0\ ; \qquad \xi_{c2} = 0.15 + \dfrac{0.072}{\rho^{0.1}} \end{cases} \tag{38}$$

Note that, for k_{ef} the density $\rho = \rho_{\mathrm{P1}} + \rho_{\mathrm{P2}}$, whereas for k_{r1} and k_{r2} $\rho = \rho_{\mathrm{r1}} + \rho_{\mathrm{P1}} + \rho_{\mathrm{P2}}$. A reference temperature T_0 is used to scale the activation energy, $T_0 = 298\,\mathrm{K}$. Quantities in this paper are all in SI units.

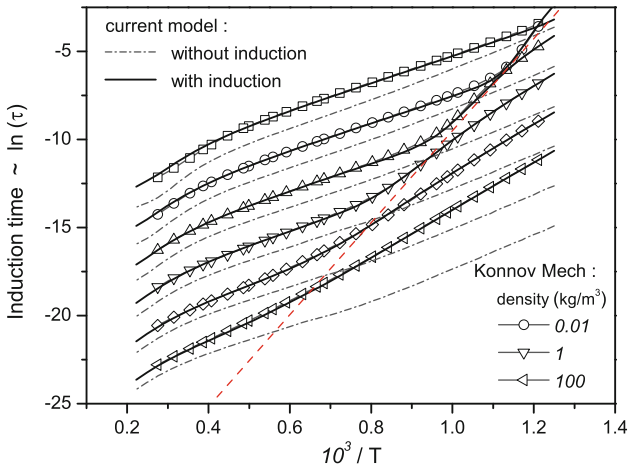

Fig. 8 Induction time of adiabatic CVE varying with initial temperature and density for stoichiometric acetylene–oxygen reaction

The rates calculated with above functions are then put back into Figs. 6 and 7 (solid lines) for comparison. In most cases, they are in good agreement with the original data.

For k_{r1} and k_{r2}, it seems that the data in low temperature region cannot be strictly subjected to a simple regularity. When fitting k_{r1L} and k_{r2L} we have emphasized on the regular part of the data, i.e. $\rho \leq 1.0\ \mathrm{kg/m^3}$, beyond which errors are produced. These errors are considered unimportant, though, for the following reasons. First, errors at low temperature will not significantly affect the time/length scale of the main heat-release zone where the high temperature rates play the dominant role. Whatever the temperature is initially it hikes up when exothermicity features. Second, the errors will not affect the time/length scale of the induction zone either, as they can be fixed up by an extra reaction (i) which is basically assigned to match the exact induction time. Third, the fitted functions are substantially valid for most cases, and the errors may be considered flaws of the rate data instead of the imperfection of the established regularity. When extracting data with Eq. (31) we have assumed [R1] $\simeq$ [R1]+[R0]. This will lead to a less evaluation of k_{r1} and k_{r2} as long as the induction reaction (i) is slow enough to survive a notable fraction of R0. Figure 8 shows the induction time of adiabatic CVE (symbols for real chemistry). Indeed there appear an evident correspondence between the low regime of induction rate (right to the dashed line) and the region of errors in Fig. 7.

Even without reaction (i) and starting directly from reactant R1, reaction (r1), (r2) and (e) have been sufficient to develop an explosion that undergoes similar process of heat-release and equilibration to those of ERM. The only crucial divergence appears at the very beginning of reaction. See Fig. 8, symbols are the CVE induction time of the Konnov mechanism, and the dash–dot lines are that of the global mechanism without reaction (i).

The induction rate k_i and reaction order s_0 is examined to make up the difference in induction. Again, noticing the step-wise feature of the induction time, the same jointing technique (Eqs. 35, 36) is employed to formulate k_i. The following settings are finally reached.

$$s_0 = 0.30 \tag{39}$$

$$k_i \begin{cases} k_{iH} = 5.5 \times 10^{-3} \rho^{0.67} T^3 \cdot \exp\left(-\dfrac{11.0\mathrm{RT}_0}{\mathrm{RT}}\right) \\ k_{iL} = 9.1 \times 10^{9} \rho^{0.63} \cdot \exp\left(-\dfrac{50.0\mathrm{RT}_0}{\mathrm{RT}}\right) \\ \mu_i = 8.0 + \dfrac{12.5}{\rho^{0.25}}; \quad \xi_{ci} = 0.79 - 0.069\ \ln \rho \end{cases} \tag{40}$$

Solid lines in Fig. 8 are the CVE induction time produced by the full steps. One can find that it agrees quite well with the reference date over the entire range studied.

With Eq. (32), Eq. (34–40), all the reaction orders and rates have been available, and the target GRM is now completed.

5.3 Validation to the reference chemistry

To validate the proposed GRM, the mechanism is applied to compute two classical problems of premixed reactive flow—adiabatic CVE and the steady laminar structure after a shock wave.

(a) Adiabatic CVE is a zero-dimensional reactive flow problem. The current GRM is derived from the data of adiabatic CVE. Here we simply put it back to revive the reaction. A 4th order Runge–Kutta method is employed to solve the ODEs.
Figure 8 demonstrates the agreement of the overall CVE induction time between the two mechanisms. To check the developing details of the reaction, temperature profiles of CVE with six different initial conditions (temperature $T_0 = 1{,}500, 2{,}000, 2{,}500\ K$ and density $\rho = 0.1$ and $10.0\ \mathrm{kg/m^3}$) are laid out in Fig. 9. Symbols are produced by the Konnov mechanism, and lines are by the current GRM. One may find that not only the time scale of different reaction stages but also the exact thermal state throughout the reaction are well depicted by this simple mechanism.

(b) The laminar structure of reaction zone after a shock wave is a one-dimensional problem which involves basic coupling of chemical reactions and gas dynamics. The flow with GRM is again solved by Runge–Kutta method, and the one with ERM is by CHEMKIN ZND program [42].
Figure 10 shows the temperature profile of the reaction zone after different strength of leading shock wave, and with two different initial pressures. The driven factor f is defined as the squared ratio of shock speed and CJ

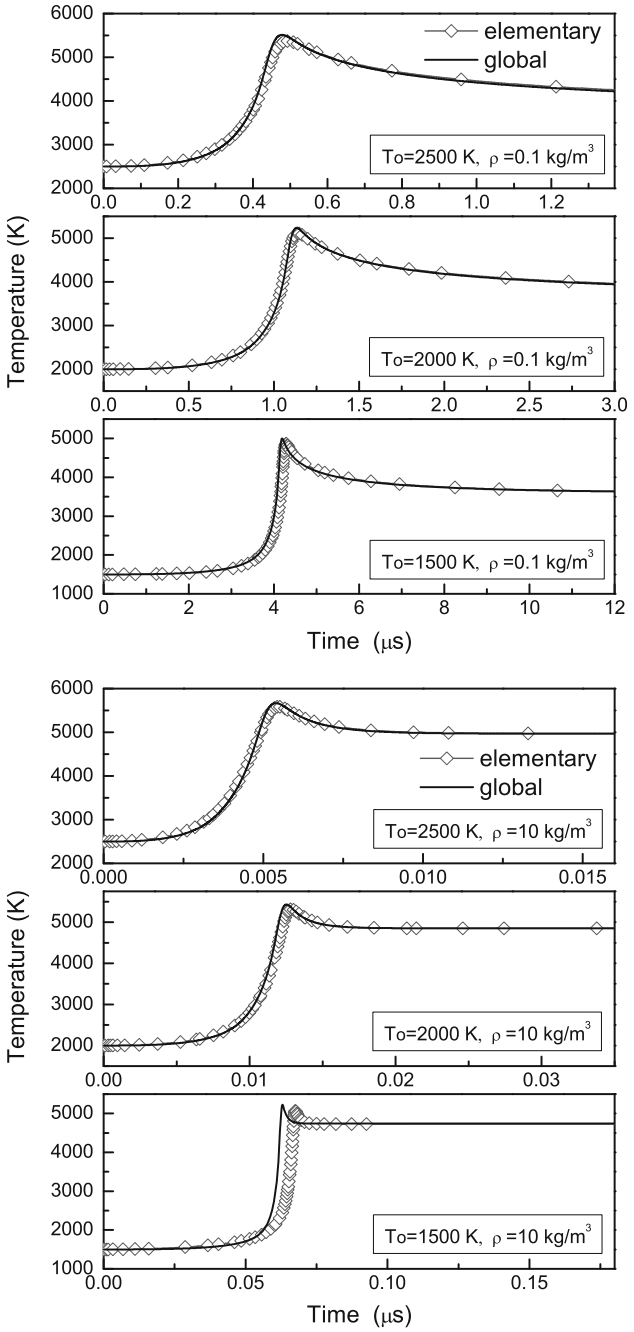

Fig. 9 Temperature profiles of adiabatic CVE in stoichiometric acetylene–oxygen mixture

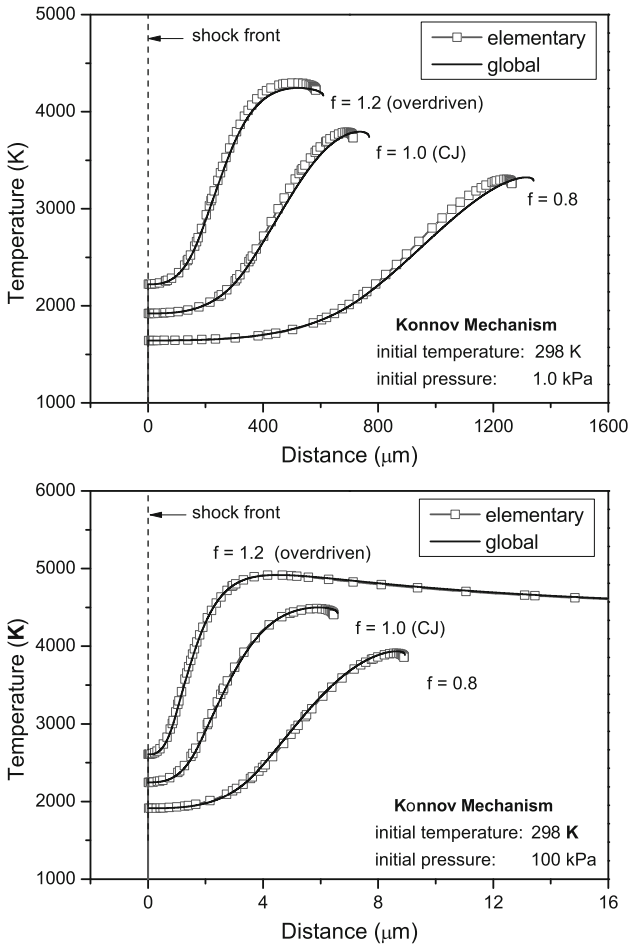

Fig. 10 Temperature profiles of the steady laminar structure after a shock wave in stoichiometric acetylene–oxygen mixture

detonation speed, $f = U_s^2/U_{\mathrm{CJ}}^2$. Tested conditions are listed in Table 3. Symbols in graphs are results of the Konnov mechanism and lines are of the current GRM. The two are found in accordance in both spacial scales and thermal state all over the test conditions.

For current mixture, the overall effect of main reaction (r1)+(r2) is exothermic, while the equilibrating reaction (e) is endothermic. According to the classical detonation theory, due to the competition effect of exothermic reaction and endothermic reaction, there is often no continuous path that can reach the final equilibrium under the CJ speed [41]. Instead, a singular point appears amid reaction, which causes a failure of the mathematical integration of the ODE. But when the detonation is overdriven enough, the singularity may vanish and the calculation may advance to the final state continuously (Fig. 10, $p_0 = 100\,\mathrm{kPa}$, $f = 1.2$). These important features are also perfectly reproduced by the current mechanism. Sharp and Falle [39] investigated the one-dimensional stability of the pathological detonation with an idealized GRM. They utilized a reaction scheme of $A \rightarrow B \rightarrow C$ which has a very similar effect as present mechanism.

6 Preliminary test in simulation of unstable detonation

As intended, the proposed GRM is applied to compute unstable detonation waves. Instead of focusing on the physics of detonation or numerical techniques, in this paper we only test the proposed GRM and demonstrate the capability as well as the potential application of it.

Table 3 initial pressure and shock wave speed tested in laminar reacting zone calculation

Initial pressure (kPa)	$f = 0.8$ (m/s)	$f = 1.0$(CJ) (m/s)	$f = 1.2$ (m/s)
1.0	1,972	2,191	2,410
100	2,185	2,428	2,671

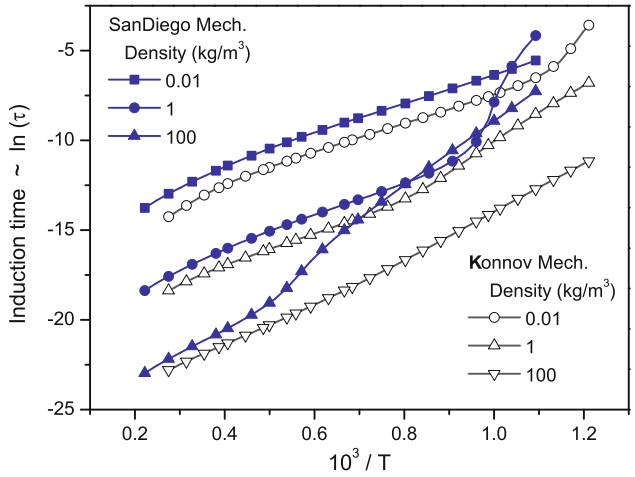

Fig. 11 Induction time of adiabatic CVE with Konnov mechanism and SanDiego mechanism (stoichiometric acetylene–oxygen mixture)

6.1 GRM for SanDiego mechanism

Before going to the simulation practice, we shall make a comparison between different mechanisms.

In above discussion, we have adopted the most complicated ERM in Table 1—the Konnov mechanism. As reported by Schultz et al. [44], even the detailed mechanisms do not always agree with each other. When it comes to the reaction of stoichiometric acetylene–oxygen, the mechanisms in Table 1 break into two camps. One of them includes the Lutz, Miller–Bowman and Konnov mechanism, and the other includes the rest. Mechanisms within each camp predict similar induction times, while between them the difference is large. The most detailed ones in each camp, i.e. the Konnov mechanism and the SanDiego mechanism, are tested. Figure 11 shows the induction time of them.

The SanDiego mechanism predicts longer induction time than the Konnov mechanism. At higher temperature and lower density, the induction time curve of the two mechanisms has a similar slope; whereas at lower temperature and higher density, the SanDiego mechanism produces a much steeper slope. This slope reflects the global activation energy of the reaction, which is known to have a significant influence on the properties of unstable detonation waves.

Directly applying these detailed mechanisms in numerical simulation to examine their effects on unstable detonation wave remain an intractable mission. The present modeling technique provides a bypass to realize such a practice at an acceptable expense. With the same reaction scheme presented in Sect. 4 and following the same fitting method in Sect. 5, a GRM for the SanDiego mechanism is also derived.

$$\begin{cases} s_0 = 0.85 \\ s_1 = s_2 = 0.8 \\ s_3 = 1.02 \end{cases} \tag{41}$$

$$k_{\mathrm{ef}} = 3.5 \times 10^{10} \rho \cdot \exp\left(-\frac{148.0\mathrm{RT}_0}{\mathrm{RT}}\right) \tag{42}$$

$$k_{\mathrm{r1}} \begin{cases} k_{\mathrm{r1H}} = 3.5 \times 10^{9} \rho^{1.2} \cdot \exp\left(-\dfrac{30.0\mathrm{RT}_0}{\mathrm{RT}}\right) \\ k_{\mathrm{r1L}} = 4.0 \times 10^{9} \rho^{1.2} \cdot \exp\left(-\dfrac{43.0\mathrm{RT}_0}{\mathrm{RT}}\right) \\ \mu_{\mathrm{r1}} = 60.0\,; \qquad \xi_{c1} = 0.18 \end{cases} \tag{43}$$

$$k_{\mathrm{r2}} \begin{cases} k_{\mathrm{r2H}} = 2.3 \times 10^{9} \rho^{1.2} \cdot \exp\left(-\dfrac{40.0\mathrm{RT}_0}{\mathrm{RT}}\right) \\ k_{\mathrm{r2L}} = 1.9 \times 10^{9} \rho^{1.2} \cdot \exp\left(-\dfrac{43.0\mathrm{RT}_0}{\mathrm{RT}}\right) \\ \mu_{\mathrm{r2}} = 60.0\,; \qquad \xi_{c2} = 0.18 \end{cases} \tag{44}$$

$$k_{\mathrm{i}} \begin{cases} k_{\mathrm{iH}} = 8.5 \times 10^{-4} \rho^{0.2} T^{3} \cdot \exp\left(-\dfrac{13.0\mathrm{RT}_0}{\mathrm{RT}}\right) \\ k_{\mathrm{iL}} = 3.5 \times 10^{9} \cdot \exp\left(-\dfrac{63.0\mathrm{RT}_0}{\mathrm{RT}}\right) \\ \mu_{\mathrm{i}} = 8.0 + \dfrac{40.0}{\rho^{0.15}}; \quad \xi_{\mathrm{ci}} = 0.925 - 0.099 \ \ln \rho \end{cases} \tag{45}$$

The two sets of GRM, written **GRM–KNV** for Konnov mechanism and **GRM–SDG** for SanDiego mechanism, are respectively tested.

6.2 Two-dimensional cellular detonation

Numerical simulation of two-dimensional cellular detonation with above two mechanisms is carried out. The inviscid fluid dynamics is solved by VAS2D [45], a Muscl–Hancock scheme solver based on quadrilateral adaptive grid. The chemical reaction is decoupled from the equation and separately solved at each grid under conservation law.

The simulation is performed in a 200×10 mm rectangular domain closed by solid walls. The computational domain is initially covered by uniform square grids of 1 mm (level 0). With a maximum adaptation level of 6, the minimum grid size is $1/2^6 \approx 0.0156$ mm. For GRM–KNV, providing the reaction zone length of the CJ detonation wave in a 2 kPa

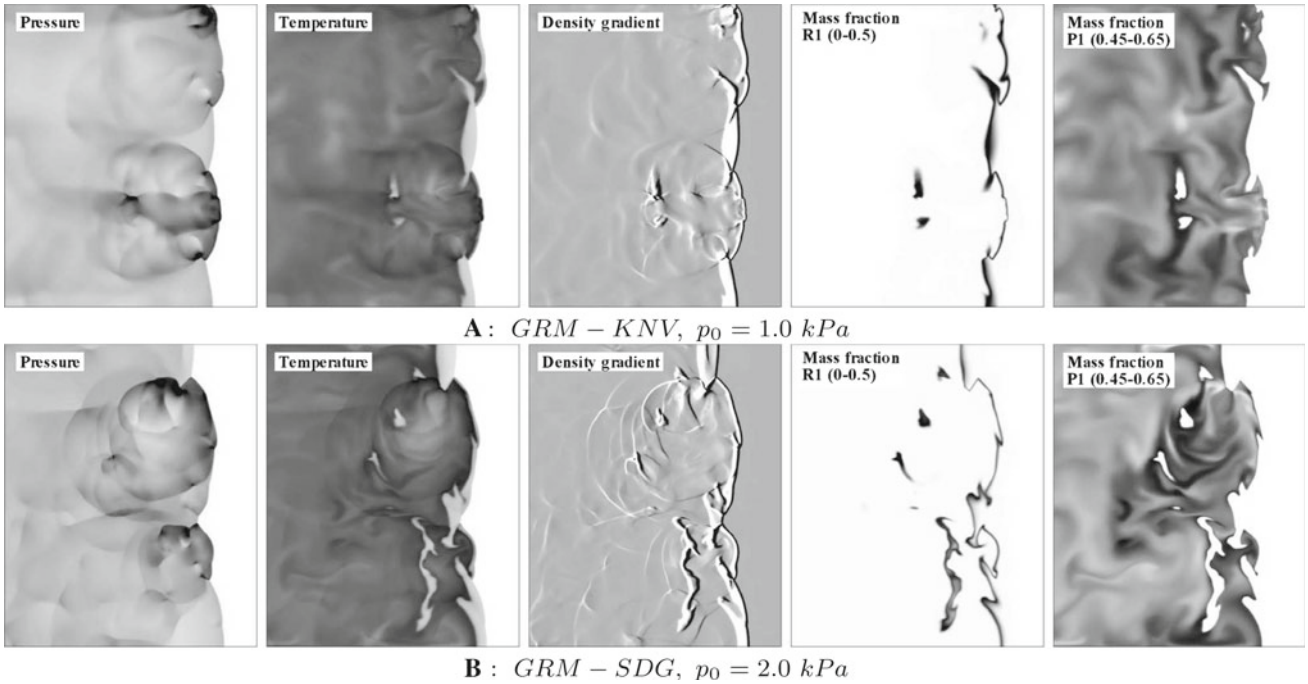

Fig. 12 A snapshot of detonation front showing contours of pressure, temperature, density gradient (numerical schlieren) and mass fractions of R1 and P1 (stoichiometric acetylene–oxygen mixture)

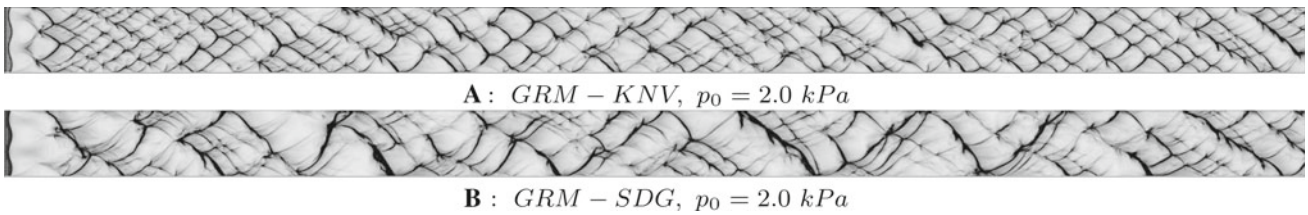

Fig. 13 Numerical soot foils for detonation initiation in stoichiometric acetylene–oxygen mixture

mixture is around 0.25 mm, we have a resolution of 8 grids per half reaction length. For GRM–SDG, the resolution is doubled.

Snapshots of typical detonation wave front produced by the two global mechanisms are shown in Fig. 12. Though both of the wave fronts are highly irregular, the triple-point features as well as the keystone-like structures are evident [40]. Two reaction products are not uniformly distributed behind the detonation. P1 surges when temperature is low. From the schlieren figures, we can see the transverse wave structures in Fig. 12b are more complicated. In Fig. 12a, two isolated low-temperature spots lag behind the detonation front. These two spots correspond to the unburned pockets which are clearly visible in images of mass fraction. In Fig. 12b, such unburned pockets are more massive. These all indicate that the detonation front produced by GRM–SDG is more violent and irregular than that of GRM–KNV.

The difference in wave front may be explained with the theory of Ng et al. [28], where a parameter χ,

$$\chi = \epsilon_I \cdot \frac{\Delta_I}{\Delta_R} \tag{46}$$

was proposed to characterize the detonation stability, with ϵ_I the normalized global activation energy, Δ_I the induction length and Δ_R the heat-release length of the ZND structure, respectively. Larger χ tends to destabilize the detonation wave. Figure 11 shows that, the SanDiego mechanism produces longer induction time than the Konnov mechanism; and the global activation energy of the former is also greater than or comparable to that of the latter. Moreover, the heat-release rates of former is also slightly larger (compare Eqs. 37–38 to Eqs. 43–44), which indicates a shorter heat-release length. All these assure the SanDiego mechanism a higher χ. Therefore the SanDiego mechanism produces a more unstable wave front.

Figure 13 shows the numerical soot foils (maximum pressure contour) of detonation waves produced by the two mechanisms. The detonation is ignited by an explosion at the left end of tube. One may note that, under same initial

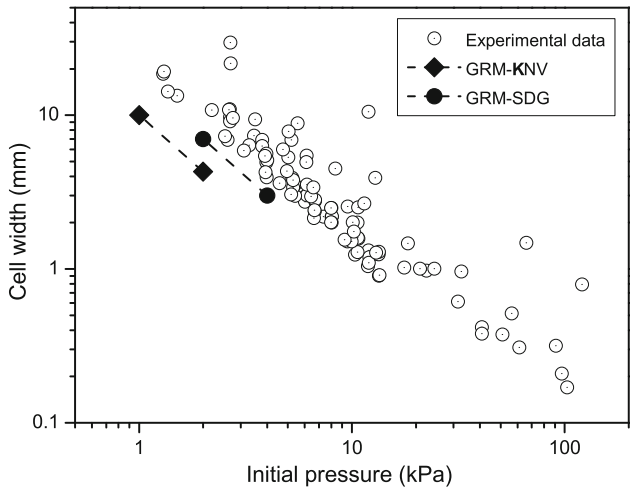

Fig. 14 Detonation cell width in stoichiometric acetylene–oxygen mixture

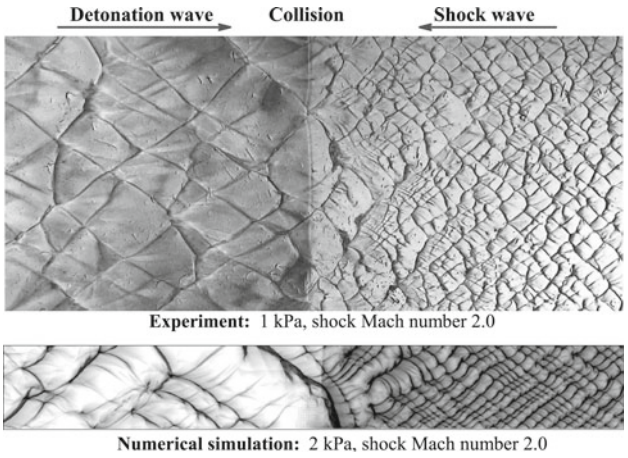

Fig. 15 Cellular patters showing the head-on collision of a shock wave and a detonation wave in mixture of stoichiometric acetylene–oxygen

pressure, the GRM–SDG produces larger cell size and more irregular cell pattern than the GRM–KNV. The averaged cell width are plotted in Fig. 14. It is found that both mechanisms underestimate the cell size, but the results of GRM–SDG are closer to the experimental data [46].

6.3 Head-on collision of detonation wave and shock wave

The head-on collision of detonation wave and shock has been investigated by Ng [47], Botros [48] and coworkers. We present here a preliminary two-dimensional numerical simulation on this process.

Cellular patterns of the detonation after the collision are shown in Fig. 15. The upper figure is the experimental result and the lower is the numerical result with GRM–SDG. As reported by [48], the detonation cell widths are correlated with the induction length calculated from the ZND model. Therefore, chemical kinetics and the gas properties are very important for simulation of this problem. From the experimental result, one may find that the cellular pattern exhibits three main variations after the interaction. First, the cell size becomes smaller; second, the cell pattern becomes more regular; third, the aspect ratio of the cell width to length becomes larger. Those variations are all depicted by the numerical result. With the same shock strength, the changing ratio of cell size of both figures also agrees.

With only four species and a less-stiff reaction system which allows a larger integration time step, the current global mechanisms prove to be economic in computation. Above numerical simulation involves a total grid number around 7×10^4. It takes about 24 h to complete such a case (detonation propagating 200 mm) on a small computer with 3.1 GHz CPU frequency. The simplest existing reaction mechanism known to author that resolves the high-temperature thermochemistry of acetylene–oxygen mixture is the 7-step mechanism [13]. Yet this mechanism costs hundred-odd hours for the same task on same computer.

7 Conclusion

The premixed reaction of stoichiometric acetylene–oxygen with detailed reaction mechanism are systematically investigated. It is found that not only the thermodynamic properties of reaction products at equilibrium but also those among reaction process can be generally described by three global species with their respective molecular weight and enthalpy data. By substituting these global species into the reaction zone of adiabatic CVE, a 4-step 4-species GRM is proposed, where the reaction rates are summarized and formulated based on an extensive study on the CVE data under varied conditions.

The proposed mechanism is validated to the detailed chemistry by calculating the CJ detonation wave, adiabatic CVE and the laminar structure after a strong shock wave. Good agreement in both reaction scales and averaged thermodynamic properties has been achieved.

The thermochemically derived global mechanism provides an economical bypass to examine the effects of detailed elementary chemistry on unstable detonation waves. For comparison, the Konnov mechanism and SanDiego mechanism are respectively summarized into simple GRMs which are then applied for numerical simulations of two-dimensional cellular detonation. Another simulation on the head-on collision of detonation and shock is also carried out to estimate the performance of the current global mechanism in a more complicated situation. Results are encouraging.

Though the current study has been focusing on the stoichiometric acetylene–oxygen mixture, brief tests on other lean

hydrocarbon mixtures have been carried out and similar features of data have been found. This indicates that the present method to derive a global reaction mechanism possesses a certain generality for premixed reactions of lean hydrocarbon mixtures.

Acknowledgments The work is supported by National Natural Science Foundation of China (Grant No. 11102204).

References

1. Lutz, A.E., Kee, R.J., Miller, J.A., Dwyer, H.A., Oppenheim, A.K.: Dynamic effects of autoignition centers for hydrogen and C1,2-hydrocarbon fuels. In: 22nd Symposium (International) Combustion, pp. 1683–1693 (1988)
2. Miller, J.A., Bowman, C.T.: Mechanism and modeling of nitrogen chemistry in combustion. Prog. Energy Combust. Sci. **15**, 287–338 (1989)
3. Konnov, A.A.: Implementation of the NCN pathway of prompt-NO formation in the detailed reaction mechanism. Combust. Flame. **156**, 2093–2105 (2009)
4. San Diego mechanism. http://web.eng.ucsd.edu/mae/groups/combustion/cermech (2006)
5. Petrova, M.V., Williams, F.A.: A small detailed chemical-kinetic mechanism for hydrocarbon combustion. Combust. Flame. **144**, 526–544 (2006)
6. Turanyi, T.: Sensitivity analysis of complex kinetic systems: tools and applications. J. Math. Chem. **5**, 203–248 (1990)
7. Turanyi, T.: Applications of sensitivity analysis to combustion chemistry. Reliab. Eng. Syst. Safe. **57**, 41–48 (1997)
8. Massias, A., Diamantis, D., Mastorakos, E., Goussis, D.A.: An algorithm for the construction of global reduced mechanisms with CSP data. Combust. Flame. **117**, 685–708 (1999)
9. Lu, T.F., Ju, Y.G., Law, C.K.: Complex CSP for chemistry reduction and analysis. Combust. Flame. **126**, 55–1445 (2001)
10. Lu, T.F., Law, C.K.: A directed relation graph method for mechanism reduction. Proc. Combust. Inst. **30**, 1333–1341 (2005)
11. Pepiot-Desjardins, P., Pitsch, H.: An efficient error-propagation-based reduction method for large chemical kinetic mechanisms. Combust. Flame. **154**, 67C81 (2008)
12. Bhattacharjee, B., Schwer, D.A.: Optimally-reduced kinetic models: reaction elimination in large-scale kinetic mechanisms. Combust. Flame. **135**, 191–208 (2003)
13. Varatharajan, B., Williams, F.A.: Chemical-kinetic descriptions of high-temperature ignition and detonation of acetylene–oxygen-diluent systems. Combust. Flame. **125**, 624–645 (2001)
14. Turanyi, A., Tomlin, A., Pilling, M.: On the error of the quasi-steady-state approximation. J. Phys. Chem. **97**, 163–172 (1993)
15. Lam, S.H., Goussis, D.A.: The CSP method for simplifying kinetics. Int. J. Chem. Kinet. **26**, 46l–468 (1994)
16. Maas, U., Pope, S.B.: Simplifying chemical-kinetics intrinsic low-dimensional manifolds in composition space. Combust. Flame. **88**, 239–264 (1992)
17. Varatharajan, B., Petrova, M., Williams, F.A., Tangirala, V.: Two-step chemical-kinetic descriptions for hydrocarbon-oxygen-diluent ignition and detonation applications. Proc. Combust. Inst. **30**, 1869–1877 (2005)
18. Sichel, M., Tonello, N.A., Oran, E.S., Jones, D.A.: A two-step kinetics model for numerical simulation of explosions and detonations in H_2–O_2 mixtures. Proc. R. Soc. Lond. A **458**, 49–82 (2002)
19. Westbrook, C.K., Dryer, F.L.: Chemical kinetic modeling of hydrocarbon combustion. Prog. Energy Combust. Sci. **10**, 1–57 (1984)
20. Jones, W.P., Lindstedt, R.P.: Global reaction schemes for hydrocarbon combustion. Combust. Flame. **73**, 233–249 (1988)
21. Andersen, J., Rasmussen, C.L., Giselsson, T., Glarborg, P.: Global combustion mechanisms for use in CFD modeling under oxy-fuel conditions. Energy Fuels **23**, 1379–1389 (2009)
22. Fickett, W., Jacobson, J.D., Schott, G.L.: Calculated pulsating one-dimensional detonations with induction-zone kinetics. AIAA J. **10**, 514–516 (1972)
23. He, L.T., Lee, J.H.S.: The dynamical limit of one-dimensional detonations. Phys. Fluids. **7**, 1151–1158 (1995)
24. Short, M., Wang, D.Y.: On the dynamics of pulsating detonations. Combust. Theory Model. **5**, 343–352 (2001)
25. Daimon, Y., Matsuo, A.: Detailed features of one-dimensional. Detonations. Phys. Fluids. **15**, 112–122 (2003)
26. Clavin, P., He, L.T.: Stability and nonlinear dynamics of one-dimensional overdriven detonations in gases. J. Fluid Mech. **306**, 353–378 (1996)
27. Short, M., Sharpe, J.: Pulsating instability of detonations with a two-step chain-branching reaction model: theory and numerics. Combust. Theory Model. **7**, 401–416 (2003)
28. Ng, H.D., Radulescu, M.I., Higgins, A.J., Nikiforakis, N., Lee, J.H.S.: Numerical investigation of the instability for one-dimensional Chapman-Jouguet detonations with chain-branching kinetics. Combust. Theory Model. **9**, 385–401 (2005)
29. Dold, J.W., Kapila, A.K.: Comparison between shock initiations of detonation using thermally-sensitive and chain-branching chemical models. Combust. Flame. **85**, 185–194 (1991)
30. Short, M., Quirk, J.J.: On the nonlinear stability and detonability limit of a detonation wave for a model three-step chain-branching reaction. J. Fluid Mech. **339**, 89–119 (1997)
31. Ng, H.D., Lee, J.H.S.: Direct initiation of detonation with a multi-step reaction scheme. J. Fluid Mech. **476**, 179–211 (2003)
32. Liang, Z., Bauwens, L.: Cell structure and stability of detonations with a pressure dependent chain branching reaction rate model. Combust. Theory Model. **9**, 93–112 (2005)
33. Liang, Z., Browne, S., Deiterding, R., Shepherd, J.E.: Detonation front structure and the competition for radicals. Proc. Combust. Inst. **31**, 2445–2453 (2007)
34. Lu, T.F., Law, C.K.: Towards accommondating realistic fuel chemistry in large-scale computations. Prog. Energy Combust. Sci. **35**, 192–215 (2008)
35. Khokhlov, A.M., Oran, E.S.: Numercial simulation of detonation initiation in a flame brush: the role of hot spots. Combust. Flame. **119**, 400–416 (1999)
36. Radulescu, M.I., Sharpe, G.J., Law, C.K., Lee, J.H.S.: The hydrodynamic structure of unstable cellular detonations. J. Fluid Mech. **580**, 31–81 (2007)
37. Radulescu, M.I., Lee, J.H.S.: The failure mechanism of gaseous detonations: experiments in porous wall tubes. Combust. Flame. **131**, 29–46 (2002)
38. Zhu, Y., Chao, J., Lee, J.H.S.: An experimental investigation of the propagation mechanism of critical deflagration waves that lead to the onset of detonation. Proc. Combust. Inst. **31**, 2455–2462 (2007)
39. Sharpe, J., Falle, S.A.E.G.: One-dimensional nonlinear stability of pathological detonations. J. Fluid Mech. **414**, 339–366 (2000)
40. Pintgen, F., Eckett, C.A., Austin, J.M., Shepherd, J.E.: Direct observations of reaction zone structure in propagating detonations. Combust. Flame. **133**, 211–229 (2003)
41. Fickett, W., Davis, W.C.: Detonation. Dover Publications, New York (1979)
42. Kee, R.J., Rupley, F.M., Meeks, E., Miller, J.A.: CHEMKIN-III: a Fortran chemical kinetics package for the analysis of gas phase chemical and plasma kinetics. Tech. Report SAND96-8216 (1996)
43. Morley, C.: Gaseq: a chemical equilibrium program for Windows. http://www.c.morley.dsl.pipex.com

44. Schultz, E., Shepherd, J.: Validation of detailed reaction mechanisms for detonation simulation. Tech. Report FM99-5, GALCIT (2000)
45. Sun, M., Takayama, K.: Conservative smoothing on an adaptive quadrilateral grid. J. Comp. Phys. **151**, 479–497 (1999)
46. Kaneshige, M., Shepherd, J.: Detonation database. Tech. Report FM97-8, GALCIT (1999)
47. Ng, H.D., Botros, B.B., Chao, J., Yang, J.M., Nikiforakis, N., Lee, J.H.S.: Head-on collision of a detonation with a planar shock wave. Shock Waves. **15**, 341–352 (2006)
48. Botros, B.B., Ng, H.D., Zhu, Y., Ju, Y., Lee, J.H.S.: The evolution and cellular structure of a detonation subsequent to a head-on interaction with a shock wave. Combust. Flame. **151**, 573–580 (2007)